



## Advancing beyond current generation dye-sensitized MgO solar cells

A. Y. EL-Etre\* , S. M. Reda , A. I. Ali , G. A. Helal

Chemistry Department-Faculty of Science-Banha University

[\\*aliyousry@hotmail.com](mailto:aliyousry@hotmail.com)

### Abstract

In this study a classical conducting glass substrate was replaced by carbon steel substrate as working electrode (anode) in dye-sensitized solar cell. Cyclic voltammetry has been used to electro deposition 1 cm<sup>2</sup> of conducting poly aniline on the surface of carbon steel substrate. Nano porous MgO oxide powder was prepared by sol-gel technique which has particle size about 28 nm. The nano powder was spread on the surface of conducting polymer to be used as PANI nano-oxide photo electrode in dye-sensitized solar cell and immersed in solution of methylene blue in water for 24 h at room temperature in the dark to be used for assembling of the DSSCs. The counter electrode is placed on top of metal oxide electrode, and then the two electrodes fastened to gather with two binder clips. The redox electrolyte solution containing 0.05M KI, and 0.05M I<sub>2</sub> in acetonitrile is injected in between the dye coated metal oxide electrode and the counter electrode. This cell was gave efficiency 0.0135%. The catalytic activity of cell toward the electrolyte was studied by cyclic voltammetry.

**Keywords:** Dye-sensitized solar cell, Electro polymerization, Polyaniline (PANI), MgO nanoparticles

Received; 2 Aug., 2017, Revised form; Aug. 2017, Accepted; Aug. 2017, Available online 1 Oct, 2017

### 1. Introduction

The worldwide demand for energy has increased with the consumption of oil reserves. The worldwide demand for energy is expected to double by the year 2050 and triple by the end of the century [1]. Due to the many advantages the photovoltaic solar power that make it one of the most promising renewable energy sources in the world [2].

A dye-sensitized solar cell (DSSC, DSC or DYSC is the third generation of solar cell [3-4] Dye-sensitized solar cell (DSSC) is widely considered as an environment-friendly photovoltaic technologies, low-cost, and high Performance [5]. In1991, the dye- sensitized solar cell (DSSC) was developed by Grätzel [6-7]. The advantages of DSSC are that it can be engineered into flexible sheets, low cost of sensitization material production, ease of fabrication and low process temperature. Due to the low cost of the overall production of DSSC, it has been expected that the DSSC type of solar cell will give a higher return of investment (ROI) when compared to Silicon based solar cell (Si-SC).[8-9].

Among the conducting polymers, polyaniline is an excellent example of  $\pi$ -conjugated polymer due to its unique electrical, electrochemical properties, easy polymerization, high environmental stability and low cost of monomer [10]. So that second approach concentrates on enhancing power conversion efficiency of DSSCs by using

electrochemical deposition technique to introduce polyaniline nanocomposites into the cell structure. The effect of type of nanocomposite on the performance of DSSC is one of our main targets of in this work.

### 2. Experimental

#### 2.1. Material

MgCl<sub>2</sub>·6H<sub>2</sub>O were purchased from (Sigma-Aldrich USA). NaOH, oxalic acid (C<sub>2</sub>H<sub>2</sub>O<sub>4</sub>) were purchased from (Sigma-Aldrich USA). Potassium Iodide (KI), Iodine (I<sub>2</sub>), Acetonitrile (CH<sub>3</sub>CN). Aniline was purchased from (Alpha). Methylene blue (MB) dye (99.95%) was purchased from Sigma-Aldrich. Fluorine doped tin oxide conducting glass (SnO<sub>2</sub>/F) (FTO) with surface resistivity 7  $\Omega$ /sq and transmittance 80-82% visible was purchased from (Sigma-Aldrich USA).

#### 2.2. Preparation methods

##### 2.2.1 Preparation of nano oxides

MgO nanoparticles is synthesized by or sol-gel technique [11-12]. In this experimental, 10 g of MgCl<sub>2</sub>·6H<sub>2</sub>O was first dissolved in 50mL of distilled water in a 1-L beaker, into which 5mL of 1N NaOH solution was added. The solution was then rapidly stirred for 4 h to generate the metal hydroxide precipitates. The metal hydroxide gel, washed several times with distilled water and dried at 60 °C for 24 h. The dried powder was finally calcinated in air under 450 °C for 2 h.

### 2.2.2. Fabrication of PANI film

The preparation of the PANI film using an electrodeposition method outlined below [13]. The electrodeposition was carried out with an electrochemical analyzer system (CHI660D, Shanghai Chenhua, Device Company, China). All experiments were implemented in a three-electrode cell, including one Pt foil as CE, one calomel Ag/AgCl electrode as a reference electrode and carbon steel with an exposed area of 1 cm<sup>2</sup> as the working electrode [14]. An aqueous solution containing 0.2M freshly distilled aniline and 1M oxalic acid was prepared. The working-electrode (anode) substrates studied were stainless steel (304 type). In the three-electrode system (Pt wire auxiliary electrode, Ag/AgCl reference electrode) and was immersed in the above solution. CV was carried out using a CHI660C electrochemical workstation (CH Instruments, USA) to deposit PANI onto the stainless steel. PANI films were fabricated by controlling the number of sweep segments with initial E =+0.2 V, high E=1.8 , scan rate = 50mVs<sup>-1</sup>. The formed PANI film was then dried at room temperature, followed by washing with ethanol Fig.(1).

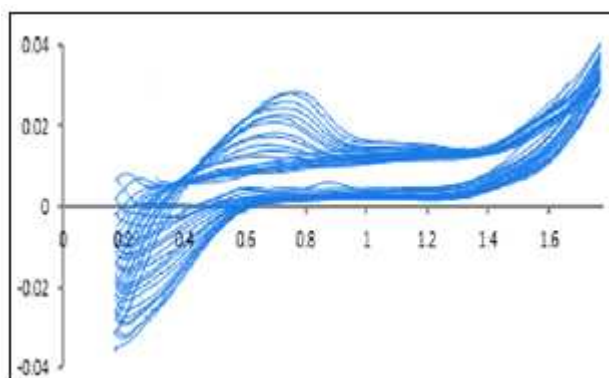


Fig (1): cyclic voltammograms of electrochemical polymerization of aniline on carbon steel substrates from aqueous solution containing 0.2 M aniline and 1M oxalic acid at scan rate 50mV /s

### 2.3. Assembly of DSSCs

#### 2.3.1 Preparation of PANI nano-oxide photoelectrode

The metal oxide has been add to the surface of PANI and immersed in methylene blue dye solution to be used for assembling of the DSSCs. The counter electrode is placed on top of metal oxide electrode, and then the two electrodes fastened to gather with two binder clips. The redox electrolyte solution is injected in between the dye coated metal oxide electrode and the counter electrode [15-16].

#### 2.3.2 Preparation of carbon counter electrode

Carbon counter electrode was prepared by sputtering a thin layer of carbon on a transparent conducting glass support using a graphite rod. Then the electrode was heated at 450 °C for 1 h, Fig.(2)

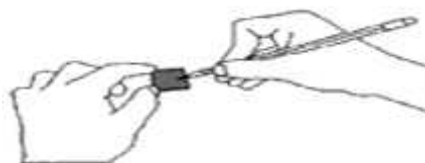


Fig (2): Preparation of carbon counter electrode

#### 2.3.3. Preparation of electrolyte

The electrolyte was prepared by mixing 0.05 M of I<sub>2</sub> and KI as redox couple in acetonitrile.

#### 2.3.4. Preparation of dye

The MB dye solution was prepared with concentration of 10<sup>-2</sup> M and stored in the dark for further applications.

#### 2.3.5. Solar cell assembly

Polyaniline film with different oxide electrodes fabricated via the electrochemical deposition method on Carbon steel for DSSCs were immersed in a 10<sup>-2</sup> M solution of methylene blue in water for 24 h at room temperature in the dark. The DSSC was assembled by a sandwiching process: the dye-coated photoanode was tightly clipped with carbon counter electrode, the electrolyte containing 0.05M KI, and 0.05M I<sub>2</sub> in acetonitrile was injected by a syringe into the space between the two electrodes [17]. The construction of the cell is represented in Fig (3).



Fig (3): The configuration of DSSC.

The characteristics of the polymeric films formed, prepared MgO, Prepared PANI nano-oxide photoelectrode and activity of electrolyte toward PANI nano-oxide photoelectrode have been studied by cyclic voltammetry , and Fourier transform infrared reflection (FTIR) techniques. Scanning electron microscopy (SEM) has been also used to study the film morphology

### 3. Results and discussion

#### 3.1. Characteristics of PANI

##### 3.1.1 FT-IR analysis

Fig (4) represents the FT-IR spectra of PANI. The band at 3420 cm<sup>-1</sup> is attributed to the N-H stretching vibrations. The band appears at 806 cm<sup>-1</sup> corresponding to out of plane bending vibration of C-H bond of p-substituted benzene ring. The bands corresponding to stretching vibrations of N-B-N and N=Q=N structures appear at 1490 and 1600 cm<sup>-1</sup>, respectively, (where -B- and =Q= stand for benzenoid and quinoid moieties in the polyaniline backbone).

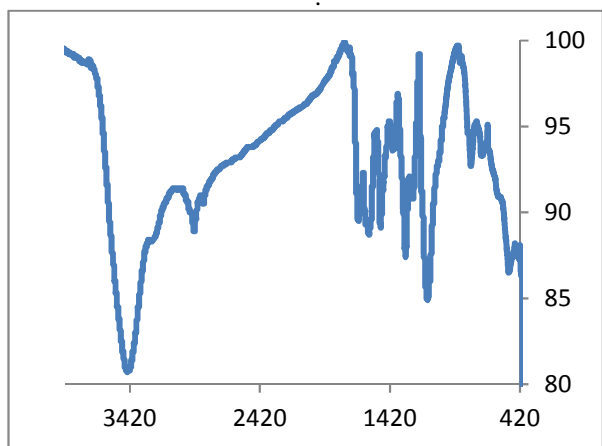


Fig (4): FT-IR spectra of PANI prepared electrochemically on carbon steel substrates from aqueous solution containing 0.2 M aniline and 1M oxalic acid

The peak appeared at 1170 cm<sup>-1</sup> corresponds to -N=Q-N+-B- which is characteristic of the protonated state. The absorption band at 1250 cm<sup>-1</sup> is associated with polaronic structure of PANI. The bands corresponding to vibration mode of N=Q=N ring and stretching mode of C-N bond appear at 1146 and 1300 cm<sup>-1</sup>, respectively. The appearances of all these bands indicate the complete polymerization of PANI by electrochemical method [18-21].

### 3.2. Characteristics of metal oxide nanoparticles

#### 3.2.1. FT-IR analysis

FT IR spectroscopy was carried out in order to ascertain the purity and nature of metal or metal oxide nanoparticles. FTIR Spectroscopy of nano metal oxide is shown in Fig(5). For the sample the broad band at 3436 cm<sup>-1</sup> and the narrow one at 1646 cm<sup>-1</sup> correspond to the stretching and bending vibrating mode of the adsorbed water. The major peak at 584 cm<sup>-1</sup> confirms the presence of Mg-O vibration.

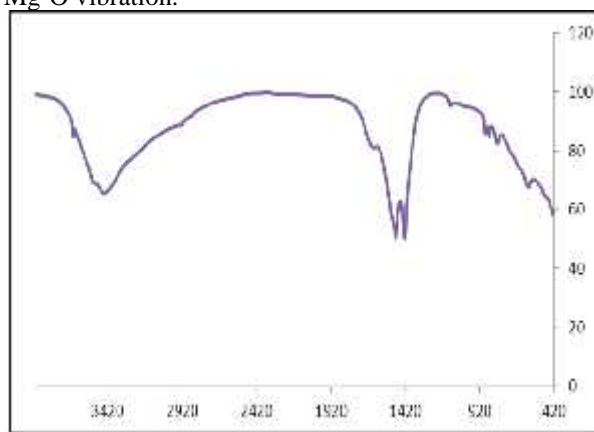


Fig (5): FTIR analysis of MgO prepared by sol-gel method

Peaks at 864 cm<sup>-1</sup> and 584 cm<sup>-1</sup> were attributed to different Mg-O-Mg vibration modes of MgO [22,23].

#### 3.2.2 XRD analysis

The crystal structure confirmation analysis was carried out by the X-ray diffraction patterns. Figure(6) shows the XRD patterns of the as-prepared products. From Fig. 1a, Five diffraction peaks were seen at 36.92°, 42.9°, 62.28°, 74.65° and 78.6°, which can be assigned to diffraction from (111), (200), (202), (311) and (222) planes, respectively, of cubic-type MgO crystal, Fig. 1c. The diffraction peaks of MgO can be matched with standard Joint Committee on Powder Diffraction Standards-JCPDS data [JCPDS file: 45-0946]. The spectrums reflect the good crystallinity for MgO nanoparticles. No characteristics peaks of Mg(OH)<sub>2</sub> and other impurities was detected in the XRD pattern.

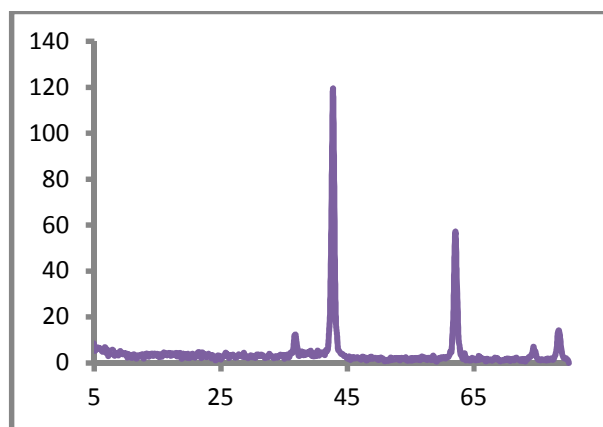


Fig (6): X-Ray Diffraction pattern of MgO prepared by sol-gel method

The average crystallite size of the as-prepared oxides was calculated using the Scherrer equation [22,23]:

$$D = \frac{0.94 \lambda}{\beta \cos \theta}$$

where *D* is the crystal size, *λ* the wavelength of X-ray (0.179 nm), *θ* half diffraction angle of peak (in degrees) and *β* the true half peak width. The average size of the as-prepared MgO determined through the (200) plane is 28 nm.

#### 3.2.3 BET analysis

The morphological characterization was performed by N<sub>2</sub> adsorption-desorption isotherms. This gives information about pore structure in our samples. Fig. (7) shows the adsorption-desorption isotherms of N<sub>2</sub> at 77 K for the prepared oxides. According to the IUPAC classification all oxides exhibited similar type I isotherms with H4 hysteresis loop in the relative pressure (*P/P*<sub>0</sub>) ranging from 0.70 to 0.98. This type of hysteresis is usually found in solids consisting of aggregates or agglomerates of particles forming slit-shaped pores with no uniform size and/or shape. The textural properties of these oxides are shown in Table 1. The result indicates that MgO has the highest BET surface area among all. The higher surface area for MgO agrees with its small particle size (28 nm) as determined from X-ray data. The higher surface area usually results in more unsaturated surface coordination sites exposed to the gas which may result in the increasing of the reducibility performance of the MgO in this study.

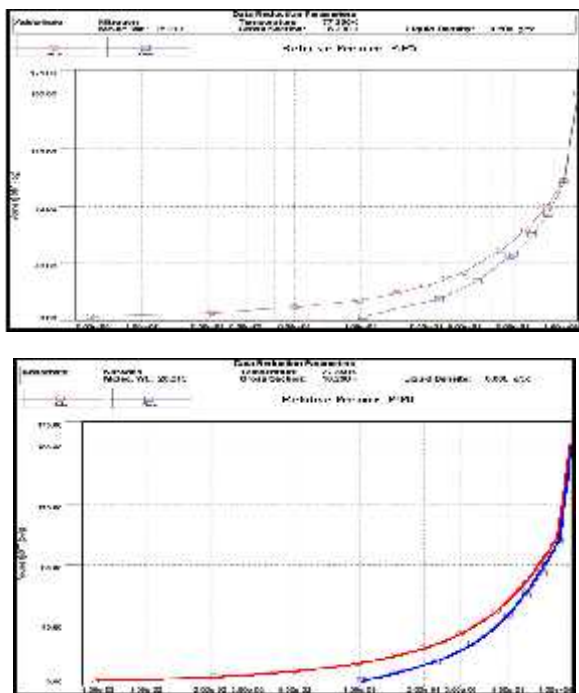


Fig (6): BET pattern of MgO prepared by sol –gel method

The mean pore radius estimated by the adsorption branch of the N<sub>2</sub> isotherm for MgO is 35 nm. This pore is mainly generated by the interstitial space between adjacent oxide nanoparticales and its high value reflects the open mesoporous architecture. The open mesoporous architecture plays an important role for the effective adsorption of MB dye. It is expected that such mesoporous structure will provide better contact for the electrolyte and channels for ion diffusion. But the small pore radius of MgO oxide make it not suitable for adsorption of MB [24].

**3.2.4 UV-Vis absorption spectroscopic analysis**

The photon absorption in many amorphous materials is found to obey the Tauc’s relation [25]:  $(\alpha h\nu)^n = A(h\nu - E_g)^m$

where (E<sub>g</sub>) the optical band gap, “A” is a constant, (α) the absorption coefficient, and (hν) the energy of the incident photon. The index n has discrete values such as 1/2, 3/2, 2 or higher depending on whether the transition is direct or indirect and allowed or forbidden [26]. In the direct and allowed cases, the index n is 1/2, whereas for the direct but forbidden cases it is 3/2. But for the indirect and allowed cases n = 2 and for the forbidden cases it is 3 or higher [27]. The optical absorption of MgO and PANI in the wavelength range of 200 nm - 900 nm has been investigated. The photon energy (hν) is plotted against (αhν)<sup>2</sup> for n = 0.5, Figs (8,9). It gives a straight line fit, which implies that the samples undergo direct transition. Then the band gap has been extracted by extrapolating the straight portion of the graph on hν axis at α = 0. The calculated values of the optical band gap for MgO and

PANI are 4.4 Ev, 2.8 Ev respectively. This is in good agreement that reported in lecture.

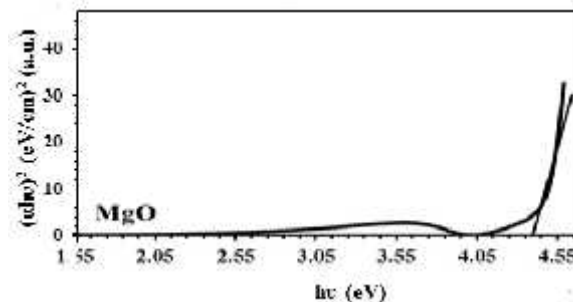


Fig (8): UV-Vis absorption spectroscopic of MgO prepared by sol-gel technique

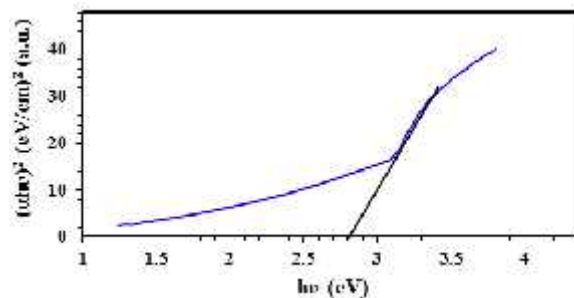


Fig (9): UV-Vis absorption spectroscopic of PANI prepared electrochemically on carbon steel substrates from aqueous solution containing 0.2 M aniline and 1M oxalic acid

**Optical properties of PANI**

The UV-Visible spectra of the prepared PANI in oxalic acid dissolved in paraffin oil shows in the figure(10) which exhibit a visible region band at ca. ranging from 300-400 nm which assigned at π\* band transition and band at ca. 900 nm polaron π\*. The band at ca. 900 nm is much clear for PANI film prepared in aqueous solution containing 1 M oxalic acid as dopant. These results ensured that the prepared PANI film is electronically conducting [28].

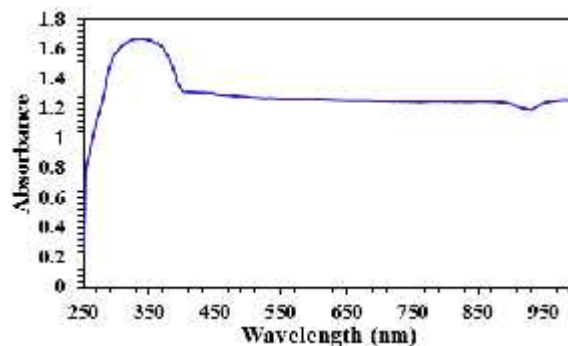


Fig (10): UV – visible spectra of PANI prepared electrochemically on carbon steel substrates from aqueous solution containing 0.2 M aniline and 1M oxalic acid

### 3.2.5 Electrical Properties

DC-conductivity of prepared oxides is measured at room temperature and shown in Fig.(11)

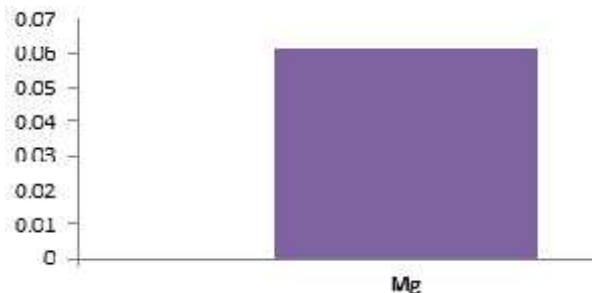


Fig (11): The electrical conductivity of MgO prepared by sol-gel technique

The electrical conductivity values was found that  $6.07 \times 10^{-8} \text{ cm}^{-1}$  for MgO,. The lowest conductivity value of MgO may be due to its highest band gap, 4.4 eV, which make a resistance for the transfer of charge carriers.

#### 3.1.3 Morphology of PANI Film

Studies on morphology of synthesized polyaniline are important for investigating the intrinsic characteristics of the polymer The morphologies of PANI were analyzed by scanning electron microscopy (SEM) and their photograph is shown in Fig (12) [29]. SEM image of electrodeposited PANi film indicates the formation of PANi. It demonstrates that all the particles of PANI are highly aggregated and irregularly shaped. This image also reveals that PANI contains some pores or voids. Figure 11b shows that the surface of the film is not smooth and contains macro-granular structure formed by the aggregation of small globular structures, which are typical ‘cauliflower’ structures. These structures refer definitely to an amorphous morphology [30].

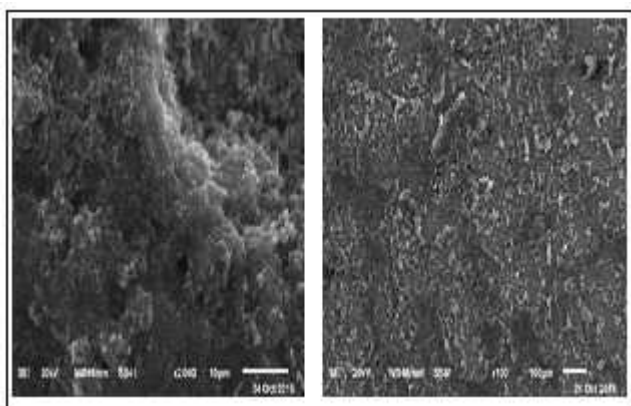


Fig (12): SEM image of polyaniline nano particles with magnification of 0.1K, 10K prepared electrochemically on carbon steel substrates from aqueous solution containing 0.2 M aniline and 1M oxalic acid

#### 2.4.6 Electro catalytic activity of the prepared electrode

Fig (13) shows the cyclic voltammograms of PANI working electrode to evaluate the catalytic activity for  $I_3^-/I^-$  in 0.05M KI and 0.05M  $I_2$  and 0.05  $Mg(ClO_4)_2$  dissolved

in acetonitrile solution in potential interval range from -3:0 V. The current peaks at the negative potential in the range from -3: 0 are assigned to the reduction reaction:  $I_3^- + 2e^- \rightarrow 3I^-$ . The votamogram curve and data indicate that prepare PANI WE is catalytically active towards  $I_3^-$  reduction [31]. The low current density explains the low efficiency of this cell.

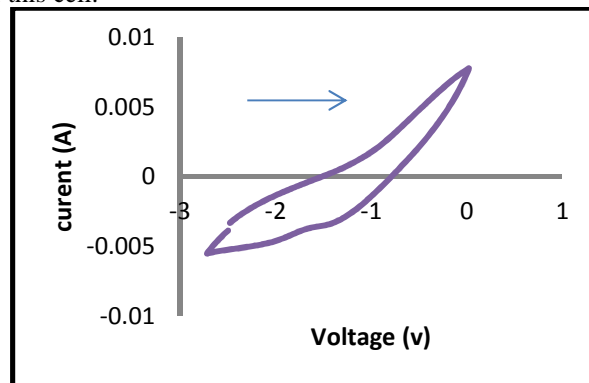


Fig (13): cyclic voltammograms of PANI photo electrodes prepared electrochemically on carbon steel substrates from aqueous solution containing 0.2 M aniline and 1M oxalic acid

Table (1) electro catalytic activity of PANI photo electrodes

Peak	Current density (mA/cm <sup>2</sup> )	potential (mV)
1	-3.5	-1.4
2	-5.0	-2.1

#### 2.4.7. Photovoltaic performance of fabricated DSSC

Fig (14) shows the photo-current-voltage curve of the DSSC with PANI-Mg oxide WE measured under irradiation of 100mW cm<sup>-2</sup>.this cell has photovoltaic parameters; short circuit current density( $J_{sc}$ ) = 0.125 mA cm<sup>-2</sup>, open circuit voltage ( $V_{oc}$ ) = 0.38 V, fill factor (FF) = 0.284 and the overall energy conversion efficiency (  $\eta$  ) = 0.0135%

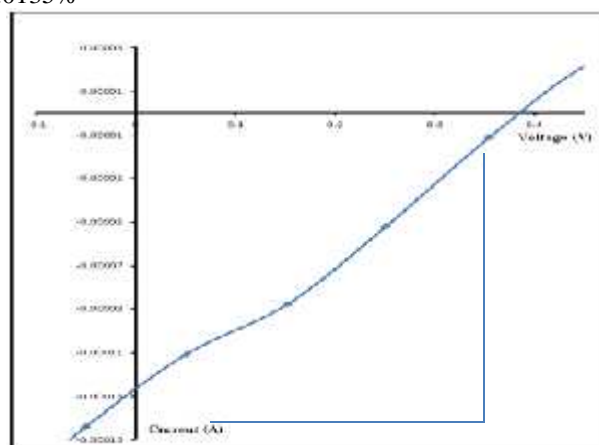


Fig (14): photocurrent density – voltage curves of DSSCS based on PANI photo electrodes prepared electrochemically on carbon steel substrates from aqueous solution containing 0.2 M aniline and 1M

Table (2): the effect of the type of metal oxides on the photovoltaic parameters of DSSCS

Jsc (mA/cm <sup>2</sup> )	Voc (V)	FF	(%)
0.125	0.38	0.284	0.0135

### References

[1] T. W. Hamann, R. A. Jensen, A. B. F. Martinson, H. V. Ryswyk and J. T. Hupp "Advancing beyond current generation dye-sensitized solar cells", *Energy & Environmental Science*,1(1), 66-78. (2008).

[2] Bagher, A, Mohammad, M, M, Abadi Vahid, and M, Mohsen. " Types of solar cells and application." *American Journal of Optics and Photonics* 3.(5) (2015): 94-113.

[3] S, Li, Y, Liu, G, Zhang, X, Zhao & J, Yin. "The role of the TiO<sub>2</sub> nanotube array morphologies in the dye-sensitized solar cells'. *Thin Solid Films*, 520(2), 689-693. (2011).

[4] Z, Lv, J Yu, H, Wu, J, Shang, D, Wang, S, Hou, Y, Fu, K, Wu and D, Zou.. "Highly efficient and completely flexible fiber-shaped dye-sensitized solar cell based on TiO<sub>2</sub> nanotube array." *Nanoscale*, 4(4), 1248-1253. (2012)

[5] J, Wu, G, Yue, Y, Xiao, M, Huang, J, Lin, L, Fan, Z, Lan and J,Y, Lin. "Glucose aided preparation of tungsten sulfide/multi-wall carbon nanotube hybrid and use as counter electrode in dye-sensitized solar cells." *ACS applied materials & interfaces*, 4(12), 6530-6536(2012).

[6] J. T. Lin, P. C. Chen, Y. S. Yen, Y. C. Hsu, H. H. Chou & M. C. P. Yeh. "Organic dyes containing furan moiety for high-performance dye-sensitized solar cells." *Organic letters*, 11(1), 97-100. (2008).

[7] J. Y. Liao, B. X. Lei, H. Y. Chen, D. B. Kuang & C. Y. Su. "Oriented hierarchical single crystalline anatase TiO<sub>2</sub> nanowire arrays on Ti-foil substrate for efficient flexible dye-sensitized solar cells." *Energy & Environmental Science*, 5(2), 5750-5757. (2012)

[8] A. Zaban, J. Zhang, Y. Diamant, O. Melemed & J. Bisquert. "Internal reference electrode in dye sensitized solar cells for three-electrode electrochemical characterizations." *The Journal of Physical Chemistry B*, 107(25), 6022-6025. (2003)

[9] P. Joshi, L. Zhang, Q. Chen, D. Galipeau, H. Fong & Q. Qiao. "Electrospun carbon nanofibers as low-cost counter electrode for dye-sensitized solar cells." *ACS applied materials & interfaces*, 2(12), 3572-3577. (2010).

Due to high gap energy of MgO about 4.4 V and low electrical conductivity of MgO about  $6.07 \times 10^{-8} \text{ cm}^{-1}$  and the photo electrode has low catalytic activity toward electrolyte I<sub>3</sub><sup>-</sup>/I<sup>-</sup> this cell has low overall energy conversion efficiency ( ) = 0.0135%.

[10] C. H. Srinivas, D. Srinivasu, B. Kavitha, N. Narsimlu & K. S. Kumar. "Synthesis and characterization of nano size conducting polyaniline." *IOSR J Appl Phys*, 1(5), 12-15. (2012).

[11] G. Moussavi & M. Mahmoudi. "Removal of azo and anthraquinone reactive dyes from industrial wastewaters using MgO nanoparticles." *Journal of Hazardous Materials*, 168(2), 806-812. (2009).

[12] Y. Zhu, J. Shi, Z. Zhang, C. Zhang & X. Zhang,"Development of a gas sensor utilizing chemiluminescence on nanosized titanium dioxide." *Analytical Chemistry*, 74(1), 120-124. (2002).

[13] Z. L. Wang, X. J. He, S. H. Ye, Y. X. Tong & G. R. Li, "Design of polypyrrole/polyaniline double-walled nanotube arrays for electrochemical energy storage." *ACS applied materials & interfaces*, 6(1), 642-647. (2013).

[14] L. Liu, H. Zhang, J. Yang, Y. Mu & Y. Wang. "Self-assembled novel dandelion-like NiCo<sub>2</sub>O<sub>4</sub> microspheres@ nanomeshes with superior electrochemical performance for supercapacitors and lithium-ion batteries." *Journal of Materials Chemistry A*, 3(44), 22393-22403. (2015).

[15] X. Xin, M. He, W. Han, J. Jung & Z. Lin. "Low-cost copper zinc tin sulfide counter electrodes for high-efficiency dye-sensitized solar cells." *Angewandte Chemie International Edition*, 50(49), 11739-11742. (2011).

[16] X. Fang, T. Ma, G. Guan, M. Akiyama, T. Kida & E. Abe. "Effect of the thickness of the Pt film coated on a counter electrode on the performance of a dye-sensitized solar cell." *Journal of Electroanalytical Chemistry*, 570(2), 257-263. (2004).

[17] N. Al-Hosiny, S. Abdallah, A. Badawi, K. Easawi & H. Talaat. "The photovoltaic performance of alloyed CdTe<sub>x</sub>S<sub>1-x</sub> quantum dots sensitized solar cells." *Materials Science in Semiconductor Processing*, 26, 238-243. (2014).

[18] L Zhang, P. Liu & Z. Su. "Preparation of PANI-TiO<sub>2</sub> nanocomposites and their solid-phase photocatalytic degradation." *Polymer Degradation and Stability*, 91(9), 2213-2219. (2006).

[19] H. Wang, Q. Hao, X. Yang, L. Lu & X. Wang. "Graphene oxide doped polyaniline for

supercapacitors." *Electrochemistry Communications*, 11(6), 1158-1161. (2009).

[20] Ö. Yavuz, M. K. Ram, M. Aldissi, P. Poddar & S. Hariharan. "Synthesis and the physical properties of MnZn ferrite and NiMnZn ferrite–polyaniline nanocomposite particles." *Journal of Materials Chemistry*, 15(7), 810-817. (2005).

[21] A. S. Roy, S. G. Hegde and A. Parveen. "Synthesis, characterization, AC conductivity, and diode properties of polyaniline–CaTiO<sub>3</sub> composites" Published online in Wiley Online Library: 24 October 2013

[22] R. Kumar, A. Sharma, N. Kishore "Preparation and Characterization of MgO Nanoparticles by Co-Precipitation Method" *International Journal of Engineering, Applied and Management Sciences Paradigms*, Vol. 07, Issue 01, September 2013

[23] P. Tamilselvi, A. Yelilarasi, M. Hema, R. A. nbarasan "Synthesis of hierarchical structured MgO by sol-gel method" Vol. 2, No. 1, 130106, April 2013

[24] A. Sabourimanesh, A. Rashidi, K. Marjani, P. Motamedara, Y. Valizadeh "Effects of Process Parameters on the Size of Nanostructure Magnesium Oxide Synthesized by a Surfactant and Ligand Assisted Wet Chemical Method Crystal Structure" *Theory and Applications*, 2015, 4, 28-34

[25] U. S. Sajeev, C. J. Mathai, S. Saravanan, R. R. Ashokan, S. Venkatachalam & M. R. Anantharaman. "On the optical and electrical properties of rf and ac plasma polymerized aniline thin films." *Bulletin of Materials Science*, 29(2), 159-163. (2006).

[26] A. A. Amer, S. M. Reda, M. A. Mousa and M. M. Mohamed "Mn<sub>3</sub>O<sub>4</sub>/graphene nanocomposites: outstanding performances as highly efficient photocatalysts and microwave absorbers." *RSC Adv.*, 2017, 7, 826.

[27] S. M. Reda & S. M. Al-Ghannam, "Synthesis and electrical properties of polyaniline composite with silver nanoparticles." *Advances in materials Physics and Chemistry*, 2(02), 75. (2012).

[28] G. G. Wallace, G. M. Spinks, L. A. P. Kane-Maguire, P. R. Teasdale, "CONDUCTIVE ELECTROACTIVE POLYMERS, Intelligent polymer system", CRC Press, Taylor & Francis Group LLC. 2009.

[29] S. Sinha, S. Bhadra, & D. Khastgir "Effect of dopant type on the properties of polyaniline." *Journal of Applied Polymer Science*, 112(5), 3135-3140. [141]. (2009).

[30] H. S. Abdulla & A. I. Abbo "Optical and electrical properties of thin films of polyaniline and polypyrrole." *Int J Electrochem Sci*, 7, 10666-10678. (2012).

[31] Q. Tai, B. Chen, F. Guo, S. Xu, H. Hu, B. Sebo & X. Z. Zhao "In situ prepared transparent polyaniline electrode and its application in bifacial dye-sensitized solar cells." *Acs Nano*, 5(5), 3795-3799. (2011).